Journal of Magnetism and Magnetic Materials ∎ (∎∎∎∎) ∎∎∎–∎∎∎

Contents lists available at ScienceDirect

Journal of Magnetism and Magnetic Materials

journal homepage: www.elsevier.com/locate/jmmm

Magnetic order of YNi_4Si-type $TbNi_4Si$

A.V. Morozkin [a,*], Fang Yuan [b], Y. Mozharivskyj [b], O. Isnard [c,d]

[a] Department of Chemistry, Moscow State University, Leninskie Gory, House 1, Building 3, GSP-2, Moscow, 119992, Russia
[b] Department of Chemistry and Chemical Biology, McMaster University, 1280 Main Street West, Hamilton, Ontario, Canada L8S 4M1
[c] Université Grenoble Alpes, Inst NEEL, BP166, F-38042 Grenoble, France
[d] CNRS, Institut NEEL, 25 Rue Des Martyrs, F-38042 Grenoble, France

ARTICLE INFO

Article history:
Received 4 November 2013
Received in revised form
6 March 2014

Keywords:
Rare-earth compound
Magnetic property
Magnetocaloric effect
Neutron diffraction
Magnetic structure

ABSTRACT

Magnetic measurements and neutron powder diffraction investigation of the magnetic structure of the YNi_4Si-type $TbNi_4Si$ compound are presented. The magnetocaloric effect of $TbNi_4Si$ is calculated in terms of the isothermal magnetic entropy change and it reaches the maximum value of –6.3 J/kg K for a field change of 0–50 kOe near T_C of ~37 K.

Below ~37 K and in a zero applied magnetic field, $TbNi_4Si$ exhibits a commensurate *b*-axis collinear ferromagnetic ordering with the **Cmm'm** magnetic space group. At 1.5 K, the terbium magnetic moment reaches the value of 8.66(6) μ_B.

1. Introduction

Recently, the orthorhombic derivative of the $CaCu_5$-type structure namely the YNi_4Si-type RNi_4Si compounds (R=Y, La–Ce, Sm, Gd–Ho) was reported [1]. Perhaps, the orthorhombic distortion of initial $CaCu_5$-type compounds is a prospective route for optimization of their magnetic and hydrogen storage properties [2–4]. Furthermore, the modification of the type structure of rare earth compounds via solid solution is useful method for the improvement of their magnetocaloric properties as clearly shown for the $Gd_5Si_2Ge_2$-based and $LaCo_{13}$-based solid solutions [5–7].

The initial $CaCu_5$-type $TbNi_5$ shows ferromagnetic ordering below T_C ~26 K with isothermal magnetic entropy change –11.5 J/kg K for a field change of 0–5 T [8]. In the zero applied field, $TbNi_5$ has a modulated ferromagnetic structure that is the superposition of the collinear ferromagnet with $\mathbf{K}_1=[0, 0, 0]$ and transverse spin wave with $\mathbf{K}_2=[0, 0, 0.018]$ in the basal plane. Two spontaneous transitions were observed in the $TbNi_5$ single crystal. At $T_C=24$ K, a second-order transition from the paramagnetic state to the incommensurate structure occurs. This is followed by a transition from the incommensurate structure to the lock-in type structure at $T_{SR}=10$ K. At 2 K an external magnetic field of 0.4 T is strong enough (when *H* is parallel to the *c*-axis) to induce a transition to a collinear ferromagnetic structure, which remains stable even when the external field is switched off [9].

One can speculate that the orthorhombic distortion achieved through the elemental substitution will influence the magnetic properties of the initial $CaCu_5$-type phases. This work aims to understand such changes in the YNi_4Si-type $TbNi_4Si$ compound, an orthorhombic derivative of the original $CaCu_5$-type $TbNi_5$ phase, through the magnetic measurements and neutron powder diffraction.

2. Material and methods

The $TbNi_4Si$ sample was prepared by arc melting of the stoichiometric amounts of Tb (99.9 wt%), Ni (99.95 wt%) and Si (99.99 wt%). The sample was annealed at 1070 K for 200 h in an argon-filled and sealed quartz tube and subsequently quenched in ice-cold water. The structure, purity and composition of the polycrystalline sample were evaluated using powder X-ray diffraction (XRD) and electron microprobe analysis. The X-ray data were obtained on a Rigaku D/MAX-2500 diffractometer ($CuK_{\alpha 1}$ radiation, $2\theta=10$–80 deg, step 0.02 deg, 1 s/step). An INCA-Energy-350 X-ray EDS spectrometer (Oxford Instruments) on the Jeol JSM-6480LV scanning electron microscope (20 kV accelerating voltage, beam current 0.7 nA and beam diameter 50 μm) was employed to perform the microprobe analyses of the sample. Signals from three points were averaged and estimated standard deviations were 1 at % for Tb (measured by L-series lines), 1 at% for Ni and 1 at% for Si (measured by K-series lines).

DC magnetization of the polycrystalline $TbNi_4Si$ sample (mass ~0.01 g) was measured on a commercial MPMS SQUID magnetometer (Quantum Design) in the temperatures range of

* Corresponding author.
E-mail address: morozkin@general.chem.msu.ru (A.V. Morozkin).

http://dx.doi.org/10.1016/j.jmmm.2014.04.057
0304-8853/

5–300 K with an applied magnetic field of 100 Oe in the zero-field-cooled and field-cooled modes. The isothermal saturation magnetization was measured for the magnetic field change from 0 till 50 kOe and for the temperature range 10–60 K with a 5 K step.

Neutron diffraction experiments were carried out at the high flux reactor of the Institut Laue Langevin (Grenoble, France). The data were collected in a zero magnetic field on the two-axis D1B powder diffractometer equipped with a 1300 cell curved detector spanning the 2θ range of 130 deg [10]. The temperature ranges were 198–64 K with a step of ~10 K and 64–1.5 K with a step of~5 K. The neutron wavelength of 2.52 Å was selected by the (002) reflection of a pyrolitic graphite monochromator and the 2θ step was 0.1 deg.

3. Theory/calculation

The unit cell data were derived from the powder XRD using the Rietan program [11,12] in the isotropic approximation at room temperature. The paramagnetic susceptibility was fitted to the Curie–Weiss law, the effective magnetic moment and paramagnetic Curie temperature were obtained from the fit [13]. Magnetocaloric effect (MCE) was calculated in terms of the isothermal magnetic entropy change, ΔS_{mag}, using the magnetization vs. field data obtained near the magnetic transition and employing the thermodynamic Maxwell equations [14]. The neutron diffraction data were refined with the FULLPROF program [15]. The "colorless" space groups and "black-white" magnetic space group [16–18] were used for the analysis of neutron diffraction data.

4. Results

4.1. Crystal structure

Both the microprobe and X-ray powder analyses showed that $TbNi_4Si$ is a single-phase sample. The microprobe analysis yielded the $Tb_{16(1)}Ni_{68(1)}Si_{16(1)}$ composition, and the X-ray powder analysis confirmed the YNi_4Si-type structure with the *Cmmm* space group. The refined lattice parameters were $a=0.50577(2)$ nm, $b=0.82131(3)$ nm, $c=0.39484(1)$ nm, $V=0.16401(4)$ nm^3 and $b/(3^{1/2}\cdot a)=0.93755(3)$ and the atomic sites were Tb1 (*2a*) [0, 0, 0], Ni1 (*4i*) [0, 0.3453(5), 0], Ni2 (*4f*) [1/4, 1/4, 1/2] and Si (*2c*) [0, 1/2, 1/2], $R_F=4.9\%$. The atomic positions for the Tb *2a* site in the *Cmmm* space group with the corresponding symmetry operators are given in Table 1.

4.2. Magnetic properties and magnetocaloric effect

The zero-field-cooled (ZFC) and field-cooled (FC) magnetization data recorded during heating in 100 Oe are shown in Fig. 1a. The FC data are indicative of a typical ferromagnet, while the ZFC data suggest presence of weak competing antiferromagnetic

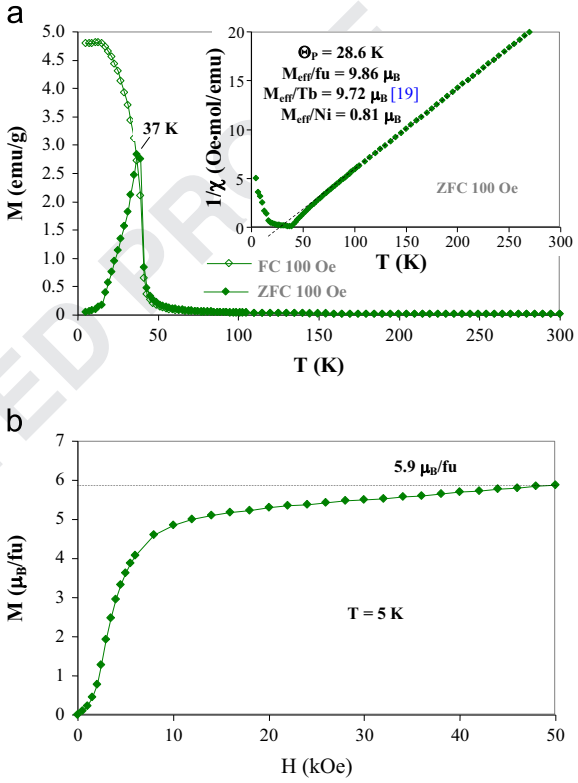

Fig. 1. (a) Magnetization and inverse magnetic susceptibility as a function of temperature, (b) magnetization vs. magnetic field at 5 K of $TbNi_4Si$.

Table 1
Atomic positions for the *2a*, *4i* and *4f* sites of the *Cmmm* [a] space group (retained by $TbNi_4Si$) with the corresponding symmetry operators and magnetic space group **Cmm′m** [b] (retained by *b*-axis collinear ferromagnetic ordering of $TbNi_4Si$) with corresponding magnetic symmetry operators.

Site	Atom	*x/a*	*y/b*	*z/c*	Symmetry operator	Magnetic symmetry operator
2a	Tb^1	0	0	0	*Pmmm* [c]	**Pmm′m** [f]
	Tb^2	1/2	1/2	1/2	*Pmmm*/[1/2 0 1/2]	**Pmm′m** × **1**/[1/2 0 1/2]
4i	$Ni1^1$	0	y	0	*Pm2m* [d]	**Pm2m** [g]
	$Ni1^2$	0	−y	0	{$\mathbf{2}_x$, $\mathbf{m}_y$, $\mathbf{2}_z$, $\bar{1}$}	$1'\times${$\mathbf{2}_x$, $\mathbf{m}_y$, $\mathbf{2}_z$, $\bar{1}$}
	$Ni1^3$	1/2	1/2+y	0	*Pm2m*/[1/2 1/2 0]	**Pm2m** × **1**/[1/2 1/2 0]
	$Ni1^4$	1/2	1/2−y	0	{$\mathbf{2}_x$, $\mathbf{m}_y$, $\mathbf{2}_z$, $\bar{1}$}/[1/2 1/2 0]	$1'\times${$\mathbf{2}_x$, $\mathbf{m}_y$, $\mathbf{2}_z$, $\bar{1}$}/[1/2 1/2 0]
4f	$Ni2^1$	1/4	1/4	1/2	$P2_1/n$ [e]	$\mathbf{P2_1'/n}$ [h]
	$Ni2^2$	−1/4	1/4	1/2	{$\mathbf{m}_x$, $\mathbf{2}_x$/[1/2 1/2 0], $\mathbf{2}_y$, $\mathbf{m}_y$/[1/2 1/2 0]}	{$\mathbf{m}_x$, $1'\times\mathbf{2}_x$/[1/2 1/2 0], $\mathbf{2}_y$, $1'\times\mathbf{m}_y$/[1/2 1/2 0]}
	$Ni2^3$	1/4	−1/4	1/2	{$\mathbf{m}_x$/[1/2 1/2 0], $\mathbf{2}_x$, $\mathbf{2}_y$/[1/2 1/2 0], $\mathbf{m}_y$}	{$\mathbf{m}_x$/[1/2 1/2 0], $1'\times\mathbf{2}_x$, $\mathbf{2}_y$/[1/2 1/2 0], $1'\times\mathbf{m}_y$}
	$Ni2^4$	−1/4	−1/4	1/2	$P2_1/n$/[1/2 1/2 0]	$\mathbf{P2_1'/n}$/[1/2 1/2 0]

[a] *Cmmm*={**1**, $\mathbf{m}_x$, $\mathbf{m}_y$, $\mathbf{m}_z$, $\bar{1}$, $\mathbf{2}_x$, $\mathbf{2}_y$, $\mathbf{2}_z$}×{**1**, **1**/[1/2, 1/2, 0]}=*Pmmm*×{1, 1/[1/2, 1/2, 0]};
[b] **Cmm′m**={**1**, $\mathbf{m}_x$, $1'\times\mathbf{m}_y$, $\mathbf{m}_z$, $1'\times\bar{1}$, $1'\times\mathbf{2}_x$, $\mathbf{2}_y$, $1'\times\mathbf{2}_z$}×{**1**, **1**/[1/2, 1/2, 0]}={**1**, $\mathbf{m}_x$, $\mathbf{2}_y$, $\mathbf{m}_z$}×{**1**, $1'\times\bar{1}$}×{**1**, **1**/[1/2, 1/2, 0]}=**Pmm′m**×{1, 1/[1/2, 1/2, 0]}
[c] *Pmmm*={**1**, $\mathbf{m}_x$, $\mathbf{m}_y$, $\mathbf{m}_z$, $\bar{1}$, $\mathbf{2}_x$, $\mathbf{2}_y$, $\mathbf{2}_z$};
[d] *Pm2m*={**1**, $\mathbf{m}_x$, $\mathbf{2}_y$, $\mathbf{m}_z$};
[e] $P2_1/n$={**1**, $\mathbf{m}_z$, $\mathbf{2}_z$/[1/2 1/2 0], $\bar{1}$/[1/2 1/2 0]};
[f] **Pmm′m**={**1**, $\mathbf{m}_x$, $1'\times\mathbf{m}_y$, $\mathbf{m}_z$, $1'\times\bar{1}$, $1'\times\mathbf{2}_x$, $\mathbf{2}_y$, $1'\times\mathbf{2}_z$}=*Pm2m*×{**1**, $1'\times\mathbf{m}_y$};
[g] **Pm2m**=*Pm2m*={**1**, $\mathbf{m}_x$, $\mathbf{2}_y$, $\mathbf{m}_z$}; and
[h] $\mathbf{P2_1'/n}$={**1**, $\mathbf{m}_z$, $1'\times\mathbf{2}_z$/[1/2 1/2 0], $1'\times\bar{1}$/[1/2 1/2 0]}={**1**, $\mathbf{m}_z$}×{**1**, $1'\times\mathbf{2}_z$/[1/2 1/2 0]}.

interactions, which can be easily overcome in small magnetic fields. The paramagnetic susceptibility of $TbNi_4Si$ follows the Curie–Weiss law in the temperature range 90–300 K (inset in Fig. 1a). The fit to the Curie–Weiss law yields a positive paramagnetic Weiss temperatures Θ_p=28.6 K and the effective moment per formula unit (M_{eff}/f.u.) of 9.86 μ_B. If Tb atoms are assumed to carry the theoretical Tb^{3+} effective moment of $\mu_{eff} = g[J(J+1)]^{1/2}\ \mu_B = 9.72\ \mu_B$ [19], Ni atoms will have an effective paramagnetic magnetic moment of 0.81 μ_B in $TbNi_4Si$. Such magnetic moment is little more than the theoretical magnetic moment of elemental Ni (0.616 μ_B) [19]. However the neutron diffraction studies do not confirm presence of magnetic moments on Ni, and thus only Tb atoms are assumed to carry localized magnetic moments. In this case, the effective magnetic moment of the Tb atoms is 9.86 μ_B, and a slight increase of ~0.14 μ_B over the theoretical value can be attributed to the polarization of conduction electrons, predominantly the Tb 5*d* ones, through the 4*f*–5*d* exchange interactions.

The magnetization vs. magnetic field for $TbNi_4Si$ at 5 K is plotted in Fig. 1b. A rapid increase in the magnetization at low fields is typical for a ferromagnet and is attributed to the domain growth. However, a subsequent slow linear increase and non-saturating behavior is indicative of the competing antiferromagnetic interactions and/or strong anisotropy. Based on the temperature-dependent magnetization data, the antiferromagnetic interactions are weak and easily overcome at fields of 100 Oe. Thus, a strong magnetic anisotropy is likely to be present in the $TbNi_4Si$ structure and does not allow the magnetic moments to be fully oriented in the magnetic field. The saturation magnetic moment reaches the value of 5.9 μ_B/Tb in 50 kOe, which is significantly smaller than the theoretical saturation moment of Tb^{3+} ($\mu = gJ\ \mu_B = 9\ \mu_B$ [19]).

The magnetocaloric effect of $TbNi_4Si$ in terms of the isothermal magnetic entropy change, ΔS_{mag}, was calculated from the saturation magnetization data (Fig. 2a). A numerical integration is performed using the following formula $\Delta S(T)_{mag} = \sum_i (M_{i+1} - M_i/T_{i+1} - T_i)\Delta H$, where ΔH is a magnetic field step and M_i and M_{i+1} are the values of magnetization at temperatures T_i and T_{i+1}, respectively [14]. The magnetic entropy change, ΔS_{mag}, for $\Delta H = 0-5$ kOe is plotted in Fig. 2b. As expected for a second order magnetic transition, ΔS_{mag} peaks around the Curie temperature and has a maximum value of −6.3 J/kg K.

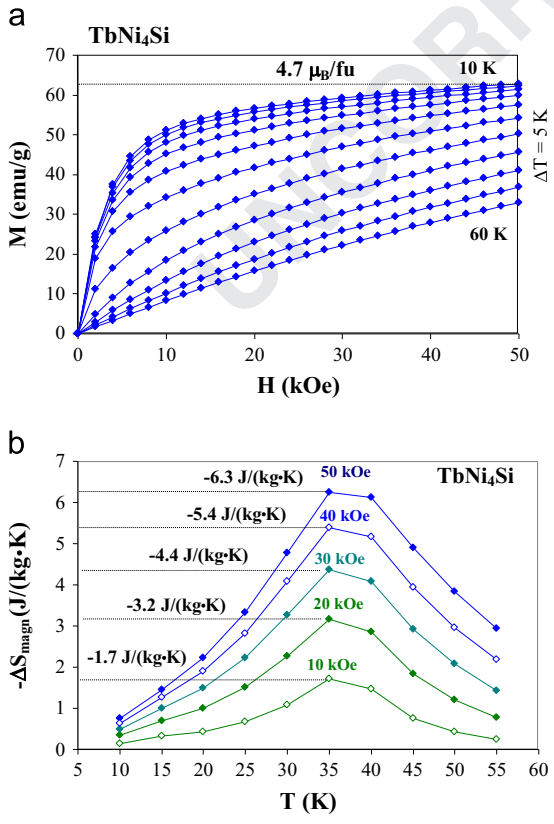

Fig. 2. (a) Magnetization vs. magnetic field and (b) the isothermal entropy change, $-\Delta S_{mag}$, of TbNi4Si around the magnetic transitions.

4.3. Magnetic structure

Above 38 K, the neutron diffraction patterns of $TbNi_4Si$ in a zero applied field correspond to the paramagnetic state, and at

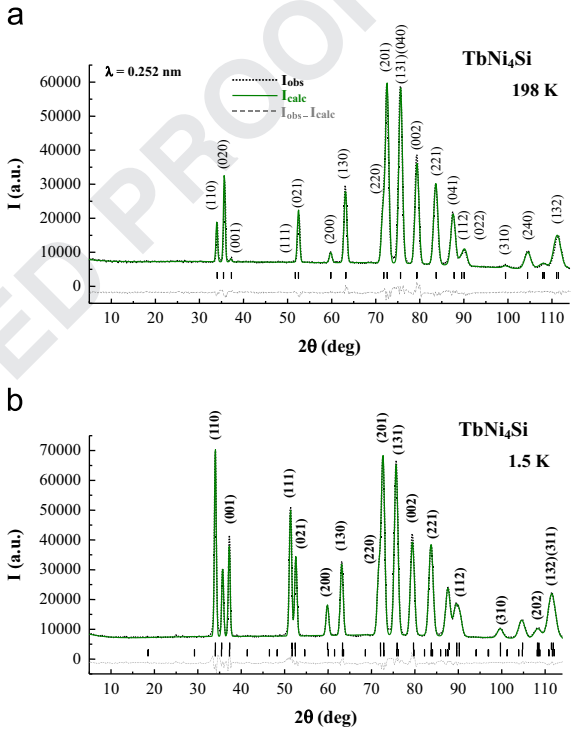

Fig. 3. Neutron diffraction patterns of $TbNi_4Si$ (a) at 198 K (paramagnetic state) and (b) at 1.5 K (*b*-axis ferromagnet with **K**=[0, 0, 0] wave vector). The first row of ticks refers to the nuclear Bragg peaks whereas the second row of lines refers to the magnetic reflections. The (*hkl*) of strongest magnetic reflections are indicated in (b).

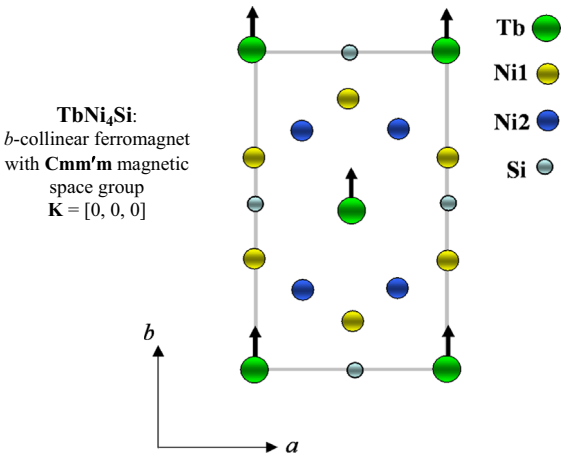

Fig. 4. The image of magnetic structure of YNi4Si-type $TbNi_4Si$ with *b*-axis collinear ferromagnetic ordering of Tb sublattice below ~38 K of **Cmm′m** magnetic space group (**K**=[0, 0, 0] wave vector).

T_C^{ND}=38 K a set of commensurate magnetic reflections with a **K**=[0, 0, 0] wave vector indicates the magnetic ordering of $TbNi_4Si$ (Fig. 3). The ordering temperature found from the neutron diffraction study is in good agreement with the value deduced from the magnetization measurements of T_C~37 K.

A commensurate *b*-axis collinear ferromagnetic model of $TbNi_4Si$ fits best with the NDP data (Fig. 4).

Within this model, the calculated magnetic moments for the Ni1 and Ni2 sublattices are close to or within the error bar (M_{Ni}~0.12(12 μ_B)) meaning that the significance of such ordered magnetic moment on Ni cannot be confirmed. The other tested commensurate variants yielded no magnetic ordering for the Ni sublattices. The *b*-collinear magnetic ordering of the Tb sublattice corresponds to the **Cmm′m** magnetic space group as shown in Table 1. The terbium magnetic moment reaches 8.66(6) μ_B at 1.5 K, a value close to the theoretical value of 9 μ_B expected for Tb magnetic moment [19] (Fig. 5 and Table 2).

The temperature-dependant changes in the lattice parameters are presented in Fig. 6. The unit cell of $TbNi_4Si$ undergoes anisotropic distortion down to temperature of ferromagnetic transition, the cell parameters decrease with $a_T/a_{298\ K} < c_T/c_{298\ K} < b_T/b_{298\ K}$; whereas $b/3^{1/2}\cdot a$ increases and below ferromagnetic ordering the cell parameters remain almost constant. As the $TbNi_4Si$ structure is an orthorhombically distorted variant of the hexagonal $CaCu_5$ structure, the $b/3^{1/2}\cdot a$ ratio can be used to estimate the degree of the distortion and its progression with temperature. The $b/3^{1/2}\cdot a$ ratio increases upon cooling from 0.93755(3) at 298 K up to 0.93832 (8) at 36 K and it stays almost constant below the Curie

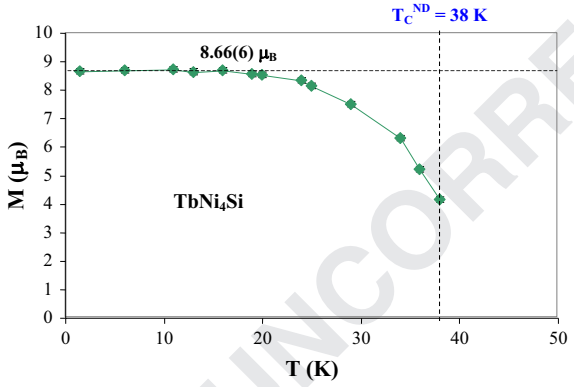

Fig. 5. The thermal evolution of Tb magnetic moment in the $TbNi_4Si$ compound from the ND data.

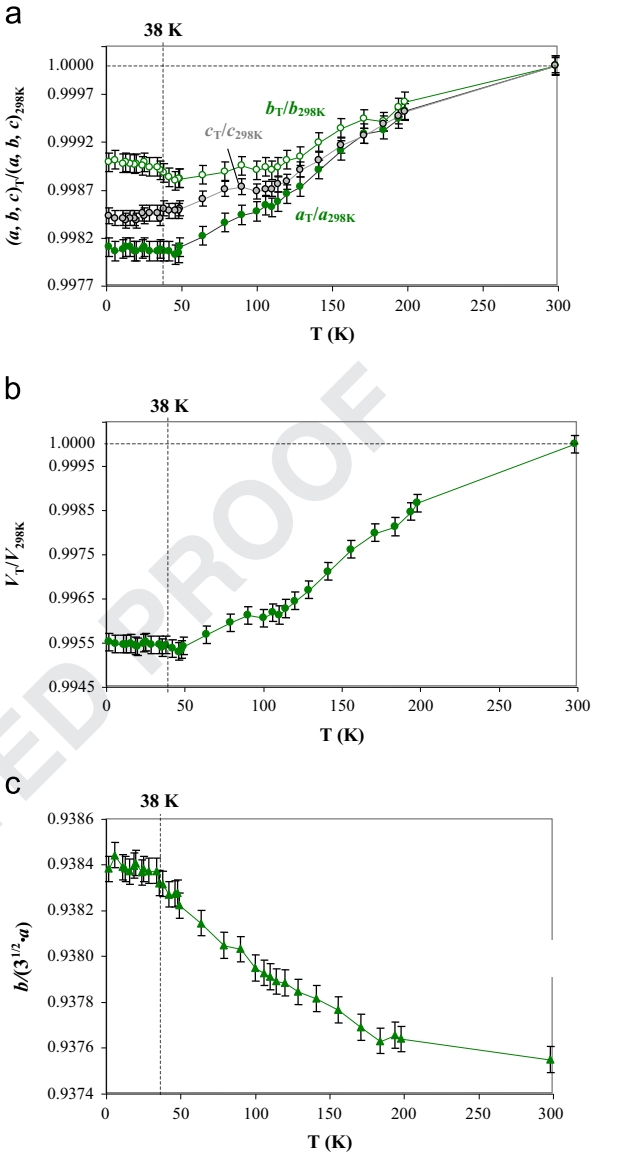

Fig. 6. Thermal variation of relative cell parameters (a) $a_T/a_{298\ K}$, $b_T/b_{298\ K}$ and $c_T/c_{298\ K}$, (b) $V_T/V_{298\ K}$ and (c) $b/(3^{1/2}\cdot a)$. Here a_T, b_T, c_T, V_T, $a_{298\ K}$, $b_{298\ K}$, $c_{298\ K}$ and $V_{298\ K}$ are cell parameters and unit cell volume of $TbNi_4Si$ at temperature *T* and at 298 K, respectively. The $b/3^{1/2}\cdot a$ ratio is the degree of the distortion of initial $CaCu_5$-type lattice.

Table 2
Crystallographic and magnetic parameters of YNi_4Si-type $TbNi_4Si$ at different temperatures: cell parameters *a*, *b* and *c*, unit cell volume *V*, $b/(3^{1/2}\cdot a)$ ratio, the atomic position of Ni1 atom y_{Ni1}[a], $\mathbf{M}_b^{K0}$ the magnetic moments of Tb, Ni1 and Ni2 along the *b*-axis with $\mathbf{K}_0$=[0, 0, 0] wave vector. Reliability factors are: R_F for the crystal structure and R_F^m for the magnetic structure.

T (K)	Cell parameters (nm)	*V* (nm^3)	$b/(3^{1/2}\cdot a)$	y_{Ni1}	R_F (%)	Atom	$M_b^{K_0}$ (μ_B)	R_F^m (%)
298[b]	*a*=0.50577(2) *b*=0.82131(3) *c*=0.39484(1)	0.16401(4)	0.93755(3)	0.3453(5)	4.9			
198	*a*=0.50543(3) *b*=0.82090(6) *c*=0.39458(2)	0.16371(8)	0.93771(7)	0.3407(2)	3.9			
1.5	*a*=0.50481(4) *b*=0.82048(6) *c*=0.39422(2)	0.16328(8)	0.93838(7)	0.3403(3)	2.9	Tb[1], Tb[2]	8.66(6)	3.3

[a] Atomic sites of YNi_4Si-type $TbNi_4Si$ (space group *Cmmm*): Tb1 (*2a*) [0, 0, 0], Ni1 (*4i*) [0, 0.3453(5), 0], Ni2 (*4f*) [1/4, 1/4, 1/2] and Si (*2c*) [0, 1/2, 1/2].
[b] X-ray data.

temperature ($b/3^{1/2}\cdot a=0.92838(7)$ at 1.5 K). The obtained value of $b/3^{1/2}\cdot a$ ratio too far from the value 1 that corresponds to the transformation of orthorhombic YN_4Si-type lattice in to hexagonal $CaCu_5$-type lattice.

5. Discussion

The saturation magnetization at 5 K and in 50 kOe yielded a magnetic moment of 5.9 μ_B per terbium atom (Fig. 1b),; whereas neutron diffraction studies at 1.5 K and in a zero applied field indicated a complete ferromagnetic ordering of $TbNi_4Si$ with 8.66 μ_B/Tb (Fig. 5). Most likely, a large magnetic anisotropy prevents a parallel alignment of all the Tb moments in the polycrystalline sample with the magnetic field even at 50 kOe.

Thus, we cannot unambiguously claim for the influence the orthorhombic distortion for magnetocaloric effect of $TbNi_5$. Meantime, orthorhombic distortion of unit cell (compression of unit cell along the *b*-orthorhombic axis) leads to the change in the Tb environment: Tb–2Tb 0.3966 nm and Tb–6Tb 0.4894 nm of $TbNi_5$ transform in to Tb–Tb2 0.39484 nm, Tb–4Tb 0.48227 nm and Tb–Tb2 0.50577 nm of $TbNi_4Si$ (the interatomic distances are given at 298 K). This distortion of unit cell leads to the disappearance of the incommensurate component in the initial $TbNi_5$ magnetic structure, increasing of temperature of magnetic ordering from 24 K up to 37 K and reorientation the terbium moments in the *ab*-plane normal to the compression of unit cell.

Thus from present experimental data the orthrhombic distortion of initial $CaCu_5$-type unit cell of $TbNi_5$ leads to the suppression of the incommensurate magnetic component, increase of Curie temperature and a decrease of magnetocaloric effect in YNi_4Si-type $TbNi_4Si$.

6. Conclusions

This work suggests possible existence of other YNi_4Si-type solid solutions with such orthorhombic distortion of initial $CaCu_5$-type unit cell. Perhaps, the orthorhombic distortion of initial $CaCu_5$-type compounds is a prospective route for optimization of their magnetic and hydrogen storage properties.

Acknowledgments

This work was supported by the Russian Fund for Basic Research through the project N° 12-03-00428-a. The Institute Laue Langevin (Grenoble, France) is warmly acknowledged for the use of the neutron diffraction beam. The author A.V.M. thanks R. Nirmala (*Indian Institute of Technology Madras*, *Chennai 600 036*, *India*) for some useful discussions.

References

[1] A.V. Morozkin, A.V. Knotko, V.O. Yapaskurt, Fang Yuan, Y. Mozharivskyj, R. Nirmala, J. Solid State Chem. 208 (2013) 9–13.
[2] K.J. Strnat, Ferromagnetic Materials, in: 131th ed.,in: E.P. Wohlfarth, K.H.J. Buschow (Eds.), Elsevier Science, North-Holland, Amsterdam, 1988.
[3] E. Burzo, A. Chelkowski, H.R. Kirchmayr, Magnetic Properties of Metals,, 248th ed., Springer-Verlag, Landolt-Bцrnstein, 1990.
[4] S.N. Klyamkin, V.N. Verbetsky, A.A. Karih, J. Alloys Compd. 231 (1–2) (1995) 479–482.
[5] V.K. Pecharsky, K.A. Gschneidner Jr., J. Magn. Magn. Mater. 167 (1997) L179–L184.
[6] V.K. Pecharsky, K.A. Gschneidner Jr, Phys. Rev. Lett. 78 (23) (1997) 4494–4497.
[7] A. Yan, K.H. Muller, O. Gutfleisch, J. Alloys Compd 450 (2008) 18–21.
[8] P.J. von Ranke, M.A. Mota, D.F. Grangeia, A.M.G. Carvalho, F.C.G. Gandra, A.A. Coelho, A. Caldas, N.A. de Oliveira, S. Gama, Phys. Rev. B 70 (2004) 134428.
[9] Seongsu Lee, A.N. Pirogov, A.A. Podlesnyak, K. Prokes, Yu.A. Dorofeef, A.E. Teplykh, I.P. Swainson, J.-G. Park, Physica B 385–386 (2006) 349–352.
[10] www.ill.eu, Yellow Book.
[11] F. Izumi, in: R.A. Young (Ed.), The Rietveld Method, Oxford University Press, Oxford, 1993, p. 13.
[12] F. Izumi, Rigaku J. 6 (1) (1989) 10–20.
[13] R.A. Levy, Principles of Solid State Physics, Academic Press, 1968. Q3
[14] A.M. Tishin, Y.L. Spichkin, The Magnetocaloric Effect and Its Applications, Institute of Physics Publishing, Bristol, Philadelphia (2003) 2003480.
[15] J. Rodriguez-Carvajal, Physica B 192 (1993) 55–69.
[16] P.S. Kireev, Introduction to the Theory Group and its Application in Solid State Physics, Moscow, High School, 1979 (In Russian).
[17] C.J. Bradley, A.P. Cracknell, The Mathematical Theory of Symmetry in Solids, Clarendon, Oxford, 1972.
[18] O.V. Kovalev, Representations of the Crystallographic Space Groups, second edition, Gordon and Breach Science Publishers, 1993.
[19] S. Legvold, Rare Earth Metals and Alloys, Ferromagnetic Materials, in: E.P. Wohlfarth (Ed.), North-Holland Publishing Company, Amsterdam, 1980, pp. 183–295.

Please cite this article as: A.V. Morozkin, et al., Journal of Magnetism and Magnetic Materials (2014), http://dx.doi.org/10.1016/j.jmmm.2014.04.057